



## City Research Online

### City, University of London Institutional Repository

---

**Citation:** Mishra, J. K., Rahman, B. M. & Priye, V. (2016). Rectangular Array Multicore Fiber Realizing Low Crosstalk Suitable for Next-Generation Short-Reach Optical Interconnects With Low Misalignment Loss. *IEEE Photonics Journal*, 8(4), pp. 1-14. doi: 10.1109/jphot.2016.2591002

This is the published version of the paper.

This version of the publication may differ from the final published version.

---

**Permanent repository link:** <https://openaccess.city.ac.uk/id/eprint/16550/>

**Link to published version:** <https://doi.org/10.1109/jphot.2016.2591002>

**Copyright:** City Research Online aims to make research outputs of City, University of London available to a wider audience. Copyright and Moral Rights remain with the author(s) and/or copyright holders. URLs from City Research Online may be freely distributed and linked to.

**Reuse:** Copies of full items can be used for personal research or study, educational, or not-for-profit purposes without prior permission or charge. Provided that the authors, title and full bibliographic details are credited, a hyperlink and/or URL is given for the original metadata page and the content is not changed in any way.

---

City Research Online:

<http://openaccess.city.ac.uk/>

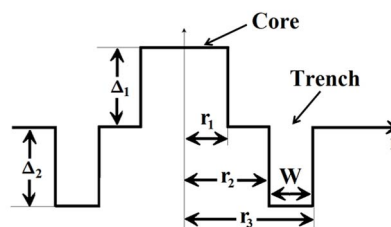
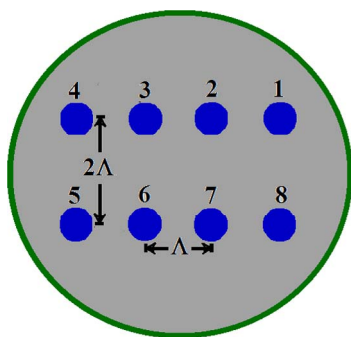
[publications@city.ac.uk](mailto:publications@city.ac.uk)

---

# Rectangular Array Multicore Fiber Realizing Low Crosstalk Suitable for Next-Generation Short-Reach Optical Interconnects With Low Misalignment Loss

Volume 8, Number 4, August 2016

Jitendra K. Mishra, Student Member, IEEE  
B. M. A. Rahman, Fellow, IEEE  
Vishnu Priye, Senior Member, IEEE



DOI: 10.1109/JPHOT.2016.2591002  
1943-0655 © 2016 IEEE

# Rectangular Array Multicore Fiber Realizing Low Crosstalk Suitable for Next-Generation Short-Reach Optical Interconnects With Low Misalignment Loss

Jitendra K. Mishra,<sup>1,2</sup> *Student Member, IEEE*,  
B. M. A. Rahman,<sup>2</sup> *Fellow, IEEE*, and Vishnu Priye,<sup>1</sup> *Senior Member, IEEE*

<sup>1</sup>Department of Electronics Engineering, Indian School of Mines, Dhanbad 826 004, India

<sup>2</sup>Department of Electrical and Electronic Engineering, City University London, London EC1V 0HB, U.K.

DOI: 10.1109/JPHOT.2016.2591002

1943-0655 © 2016 IEEE. Translations and content mining are permitted for academic research only.

Personal use is also permitted, but republication/redistribution requires IEEE permission.

See [http://www.ieee.org/publications\\_standards/publications/rights/index.html](http://www.ieee.org/publications_standards/publications/rights/index.html) for more information.

Manuscript received February 29, 2016; revised July 5, 2016; accepted July 6, 2016. Date of publication July 18, 2016; date of current version July 26, 2016. This work was supported by the European Commission under the AREAS+ Erasmus Mundus mobility programme. Corresponding author: J. K. Mishra (e-mail: jkmishra.ism@gmail.com).

**Abstract:** Toward the next-generation exa-scale short-reach optical interconnects (OIs) supporting large-capacity data transmission, a compact computer-compatible 8-core heterogeneous trench-assisted multicore fiber (TA-MCF) is proposed, in which cores are arranged in a rectangular array. To analyze the crosstalk (XT) between adjacent cores of TA-MCF OI, a rigorous full-vectorial  $\mathbf{H}$ -field finite element method (FEM) and coupled power theory are applied. The impact of various trench design parameters on the mode-coupling coefficient  $C_{mn}$  and the coupling length  $L_c$  is discussed in detail. An accurate explicit condition for the achievement of low XT in an 8-core heterogeneous TA-MCF OI is obtained through numerical simulations. A rigorous modal solution approach based on the computationally efficient FEM and the least squares boundary residual method is employed to analyze the coupling loss caused by the misalignment to a butt-coupled TA-MCF OI.

**Index Terms:** Optical interconnects (OIs), multicore fibers (MCFs), crosstalk (XT), coupling loss.

## 1. Introduction

Optical interconnect (OI) is advocated as a promising technology to overcome the capacity requirements of futuristic data centers, core routers, digital cross connect systems, and on-chip integrated photonic systems [1]. So far, bandwidth scaling has been sustained by mature technologies of fiber ribbons or individual fibers but may not be enough to exploit huge optoelectronic bandwidth disparity existing between the requirement and availability in the forthcoming era of big data and high-speed Internet traffic [2]. To combat the explosive growth in data volume requirement of next-generation high-performance short-reach OIs, a novel means for signal transmission is currently subject to intense research [3]. OI configuration based on multicore fiber (MCF) has recently attracted attention as a potential approach

to respond to the severe requirements of future short-reach optical transmission systems [4]. The space division multiplexing (SDM) technology realized by MCF is expected to overcome the imminent capacity crunch of short-reach OIs [5]. Besides increasing the transmission capacity, MCF OI shows promise for coping with the cable size limitation in bandwidth intensive box-to-box, rack-to-rack, board-to-board and chip-to-chip interconnect applications which necessitate high fiber count and high density cable [6]. Among other motivations, MCF with SDM is also less susceptible to optical power limitations imposed by the fiber non-linear effects due to small power concentration per core [7]. However, suppression of intercore cross-talk (XT) is a primary concern in interconnection technology for efficient usage of MCF as OI [8]–[10].

Recently, various types of MCFs such as homogeneous MCFs [11], heterogeneous MCFs [12], and hole assisted MCFs [13] have been intensively investigated for high-capacity long-distance transmissions with the goal of suppressing the XT between the adjacent cores. Furthermore, it has also been proved that trench-assisted MCF (TA-MCF) realizes low intercore XT with high core density comparing to MCF with step-index profile [14]–[18]. Most of the results reported pertain to hexagonal or ring structures of MCF but their use as an OI is relatively less investigated. By keeping this in mind, a holey microstructured MCF based OI is recently proposed to realize low XT with dense core arrangement [4]. Furthermore, a ring structure of an 8-core homogeneous TA-MCF has been recently published for OI applications [19]. The hexagonal geometry of MCF can also support 2-D arrays of low cost vertical-cavity surface emitting lasers [20]. Although, hexagonal or ring arrangement of cores in MCF are more tightly packed but these are not compatible with number of parallel lanes in data buses required in high performance computers, as well as on-chip integrated photonic systems. For such specific applications, rectangular array 8-core homogeneous MCF has been recently reported for OI applications [21], but homogeneous step-index MCF will result in a large XT between adjacent cores [22]. Furthermore, research on 8-core heterogeneous MCF has also been published recently [6], [23]. So, in order to minimize the intercore XT, rectangular arrayed heterogeneous TA-MCF can be a viable solution. However, to the best of our knowledge there has been no report yet on the rectangular arrayed heterogeneous TA-MCF for short reach OI applications.

The next daunting issue associated with the practical use of MCF as OI is the coupling of MCF to standard single-mode single core fibers (SCFs). So far, several fan-in fan-out (FIFO) schemes have been proposed, such as fiber bundled type [24], physical contact method [25], and coupling with lens optics [26]. Even though these proposals exhibited high coupling efficiency, their large size and mechanical instability would be concerns. In order to realize a precise alignment between MCF and SCF, grating coupler array based FIFO [27] and V-groove type FIFO [28] have been recently reported. However, to obtain a low-loss coupling is particularly challenging due to the versatile core distribution geometries of MCFs. In this context, laminated polymer waveguide has been designed to allow efficient butt-coupling to the seven-core MCF [29]. However, it has also been suggested that the least squares boundary residual (LSBR) [30] method would be more efficient and accurate to use to determine the modal excitation coefficients at the butt-coupled junctions. As far as we know, there has been no report applying LSBR method to a butt-coupled MCF OI.

In this paper, an 8-core heterogeneous TA-MCF with rectangular arrangement is being proposed to meet the requirements of next-generation exa-scale short reach OIs and on-chip integrated photonic systems. The effects of quantitative and qualitative trench design parameters on the mode coupling coefficient  $C_{mn}$  in the 8-core TA-MCF are investigated by using a rigorous full-vectorial **H**-field finite element method (FEM) [31]. The optimal trench design is based on suppressing the intercore XT in a TA-MCF OI. Subsequently, the modal solution approach based on the numerically efficient FEM [31] and the LSBR [30] method have been used to assess the effect of misalignments between MCF and SCF. The influence of butt-coupled TA-MCF OI on coupling loss is also discussed and compared with the excited modal coefficients at the butt-coupled junction of step index MCF OI.

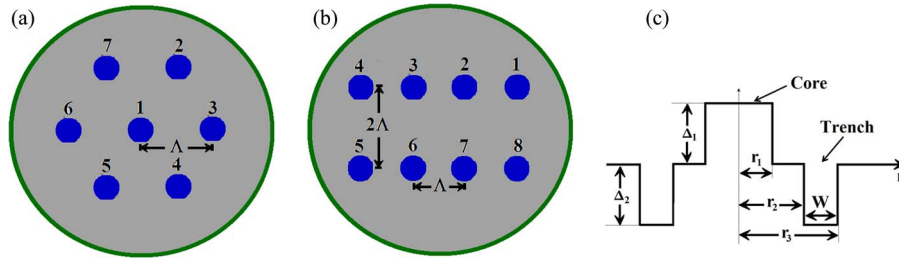


Fig. 1. Schematics of (a) a 7-core MCF, (b) an 8-core MCF, and (c) a trench-assisted index profile.

## 2. Theory

Fig. 1(a) shows a schematic cross section of hexagonally arranged 7-core MCF with a step-index profile. The design concept model of proposed MCF based OI, inside of which cores are arranged in rectangular arrays, as shown in Fig. 1(b) and the index profile of a core with trench, is shown in Fig. 1(c). All cores in TA-MCF OI are arranged with core to core pitch ( $\Lambda$ ) and distance between the two rows is  $2\Lambda$ . In Fig. 1(c),  $r_1$ ,  $r_2$ ,  $r_3$ ,  $\Delta_1$ ,  $\Delta_2$ , and  $W$  represent the core radius, the distance between the center of core and the inner edge of trench, the distance between the center of core and the outer edge of trench, the relative refractive-index difference between core and cladding, the relative refractive-index difference between trench and cladding, and the width of the trench layer, respectively.

### 2.1. Calculation of $C_{mn}$ and XT Between TA-MCF OI Cores

In order to obtain the XT between two adjacent cores in TA-MCF, coupled power theory [10] is employed, but before that the value of mode coupling coefficient  $C_{mn}$  between two neighboring cores of MCF OI with trench index profile is investigated first. The expression of coupling coefficient between two cores is given as [32]

$$C_{mn} = \frac{\omega \varepsilon_0 \int_{-\infty}^{+\infty} \int_{-\infty}^{+\infty} (N^2 - N_n^2) E_m^* \cdot E_n dx dy}{2 \sqrt{\int_{-\infty}^{+\infty} \int_{-\infty}^{+\infty} (E_{mx} H_{my}^* - E_{my} H_{mx}^*) dx dy} \cdot \sqrt{\int_{-\infty}^{+\infty} \int_{-\infty}^{+\infty} (E_{nx} H_{ny}^* - E_{ny} H_{nx}^*) dx dy}} \quad (1)$$

where  $\omega$  is an angular frequency of sinusoidally varying electromagnetic fields, and  $\varepsilon_0$  is the permittivity of free space. The pair  $m$  and  $n$  is either (1, 2) or (2, 1).  $E$  and  $H$  represent the electric and magnetic fields respectively. The refractive-index distribution in the entire coupled region is expressed as [32]

$$N^2 = N_1^2 + N_2^2 - n^2 \quad (2)$$

where  $N_1$  and  $N_2$  represent the refractive index distribution of each core with trench index profile, and  $n$  represents the refractive index distribution outside the cores respectively.  $N^2 - N_1^2$  is zero except inside the core 1, while  $N^2 - N_2^2$  is zero everywhere except inside core 2 [32].

A rigorous full-vectorial  $\mathbf{H}$ -field finite element method (FEM) [31] is used in this work to calculate the mode coupling coefficient  $C_{mn}$ . The FEM, based on the vector- $\mathbf{H}$ -Field formulation has been established as one of the most accurate and numerically efficient approaches to obtain the modal field profiles and mode propagation constants of the arbitrarily-shaped waveguides with curved boundaries [31]. The full-vectorial formulation is based on the minimization of the full  $\mathbf{H}$ -field energy functional [31]

$$\omega^2 = \frac{\int \int [(\nabla \times \mathbf{H})^* \cdot \varepsilon^{-1} (\nabla \times \mathbf{H}) + \rho (\nabla \cdot \mathbf{H})^* (\nabla \cdot \mathbf{H})] dx dy}{\int \int \mathbf{H}^* \cdot \mu \mathbf{H} dx dy} \quad (3)$$

where  $\mathbf{H}$  is the full-vectorial magnetic field,  $*$  denotes a complex conjugate and transpose,  $\omega^2$  is the eigenvalue ( $\omega$  being the angular frequency),  $p$  is a weighting factor for the penalty term to eliminate spurious modes, and  $\varepsilon$  and  $\mu$  are the permittivity and permeability tensors, respectively. The mode coupling coefficients between the cores are used to calculate the power coupling coefficient [10]. Analytical approach based on exponential autocorrelation function and coupled power theory is employed to realize the accurate evaluation of intercore XT [10]. The power coupling coefficient based on an exponential autocorrelation function can be given as [10]

$$h_{mn} = \frac{2K_{mn}^2 d_c}{1 + (\Delta\beta_{mn} d_c)^2} \quad (4)$$

where  $m, n$  represent the core  $m$  and  $n$ ;  $K_{mn}$  is the average value of mode coupling coefficient  $C_{mn}$  and  $C_{nm}$ ;  $d_c$  is the correlation length; and  $\Delta\beta_{mn}$  is the propagation constant difference between the fundamental modes of cores  $m$  and  $n$ . Here, considering the bend-induced random perturbations that can occur while practical situation or during their usage as interconnects, the MCF is divided into finite segment of correlation length  $d_c$ . In order to calculate the average value of intercore XT,  $d_c = 0.05$  m is used in this work, because this value agreed better with the measured results [9]. The XT between two cores of TA-MCF OI over a length  $L$  is estimated by the coupled power theory as [10]

$$XT = \tanh(\bar{h}_{mn}L) \quad (5)$$

where  $\bar{h}_{mn}$  represents the average power coupling coefficient. The full-vectorial field obtained by using the  $\mathbf{H}$ -field based FEM is utilized to calculate  $C_{mn}$  and  $h_{mn}$  and, finally, the XT.

## 2.2. Calculation of Coupling Loss due to Misalignment

A powerful numerical approach, the LSBR [30] method is employed to analyze the power coupling between a MCF OI and a standard SCF. When butt-coupling to a MCF OI, it is desirable that the beam divergence from the MCF is matched to the spot size of the standard SCF for precise core alignment and low loss coupling. To undertake the analysis proposed, computationally efficient vector FEM [31] is used to obtain the modal field profiles over the cross section of the discontinuity plane. Subsequently, the LSBR method has been used here, which rigorously satisfies the continuity of the tangential electric and magnetic fields at the junction interface in a least-squares sense, to find the transmission and reflection coefficients at the butt-coupled junction interfaces. The LSBR method looks for a stationary solution to satisfy the continuity conditions by minimizing the error energy functional  $J$ , as given by [30]

$$J = \int_{\Omega} |E_t^I - E_t^{II}|^2 + \alpha Z_0^2 |H_t^I - H_t^{II}|^2 d\Omega \quad (6)$$

where  $Z_0$  is the free-space impedance;  $E_t^I, E_t^{II}, H_t^I,$  and  $H_t^{II}$  are the transverse components of the electric and magnetic fields in side I and side II; and  $\alpha$  is the dimensionless weighting factor to balance the electric and magnetic components of the error functional  $J$ . The integration is carried out at the junction interface  $\Omega$  between a straight MCF OI and a conventional SCF.

## 3. Numerical Results

Before calculating the  $C_{mn}$  values, numerical accuracy of the  $\mathbf{H}$ -field based finite element modal solutions is tested. The variations of the effective index,  $n_{\text{eff}}$  with the number of mesh divisions  $N$  used is shown in Fig. 2 for the fundamental mode of a SCF (see the inset of Fig. 2) designed with core refractive index  $n_g = 1.4551$ , cladding refractive index  $n_c = 1.45$ , and core diameter  $8.9 \mu\text{m}$  at the operating wavelength of  $1550 \text{ nm}$ . Here, in both the transverse directions, equal number of mesh,  $N$  are used. The SCF is simulated by exploiting the full, half (one-fold symmetry), and quarter (two-fold symmetry) structures with the same value of  $N$  in both the transverse

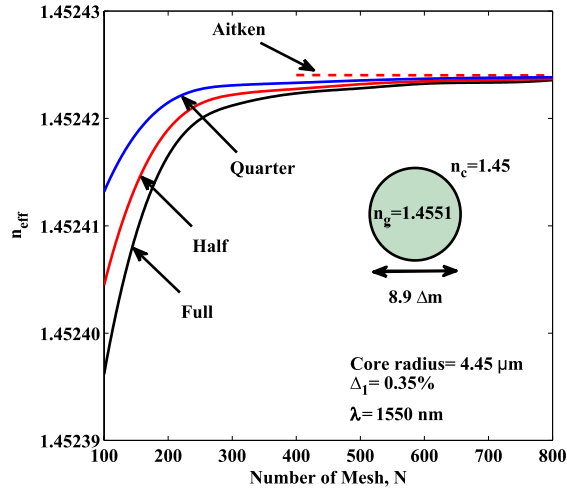


Fig. 2. Variations of  $n_{\text{eff}}$  of the fundamental mode with the number of mesh in both the transverse directions.

directions. From the results depicted in Fig. 2, it can be inferred that, as the value of  $N$  increases,  $n_{\text{eff}}$  first increases rapidly and then reaches a constant value asymptotically. From Fig. 2, it is noted that when one-fold symmetry is used, shown by a red solid line, convergence is much faster than when the full structure is simulated, shown by a black solid line. However, it can be easily observed that as mesh refinement is carried out for two-fold symmetry,  $n_{\text{eff}}$  rapidly converge to their exact solutions, as shown by a blue solid line. It should be noted that when a  $100 \times 100$  mesh is used  $n_{\text{eff}}$  is accurate to fourth decimal place for two-fold symmetry, and the accuracy is increased to 6th decimal place when mesh size is increased to  $400 \times 400$ . A powerful Aitken's extrapolation technique [33] can also be used to improve the solution accuracy of modal solution for this SCF structure. From three successive values of  $n_{\text{eff}}$  with fixed geometric mesh division ratio in both the transverse directions of SCF, final solutions can be extrapolated for a possible infinite mesh refinement as given as

$$n_{\text{eff}}^{\infty} = n_{\text{eff}(r+1)} - \frac{[n_{\text{eff}(r+1)} - n_{\text{eff}(r)}]^2}{n_{\text{eff}(r+1)} - 2n_{\text{eff}(r)} + n_{\text{eff}(r-1)}}. \quad (7)$$

Aitken's extrapolated values of  $n_{\text{eff}}^{\infty}$  for two-fold symmetry are plotted in Fig. 2 by a red-dashed line. Using (7), for instance, we calculate Aitken's value from three  $n_{\text{eff}}$  values of 1.45241317, 1.45242148, and 1.45242332 for  $N = 100, 200,$  and  $400$ , respectively. From these three values, the extrapolated more accurate value is obtained as 1.452424045. Fig. 2 clearly demonstrates the advantage of using Aitken's extrapolation technique as shown by a red dashed line.

In order to demonstrate the accuracy of mode coupling coefficient  $C_{mn}$ , numerical simulations based on the rigorous vector **H**-field FEM [31] is used to calculate the coupling coefficient between adjacent and non-adjacent cores in 7-core MCF. The cross section of the homogeneous 7-core MCF with step index profile is shown in Fig. 1(a). For hexagonal MCF, individual cores are of radius  $r_1 = 4.5 \mu\text{m}$  with refractive index of core  $n_g = 1.447$  and cladding refractive index  $n_c = 1.444$ , are taken, identical as in [14], to make a fair comparison. The operating wavelength  $\lambda$  of the optical signal is 1550 nm. The variations of the  $C_{mn}$  between adjacent and non-adjacent cores in hexagonal structure of 7-core MCF with core to core pitch  $\Delta$  are shown in Fig. 3(a). The dashed line represents the results of coupling coefficient between adjacent ( $C_{12}$ ) and non-adjacent ( $C_{24}$  and  $C_{25}$ ) cores, which were reported in [14]. On the other hand, solid line represents the results of  $C_{12}, C_{24},$  and  $C_{25}$  obtained by using the **H**-field based FEM [31]. It can be observed from Fig. 3(a), the  $C_{mn}$  estimations based on the rigorous vector **H**-field FEM are in good agreement with the results reported in [14].

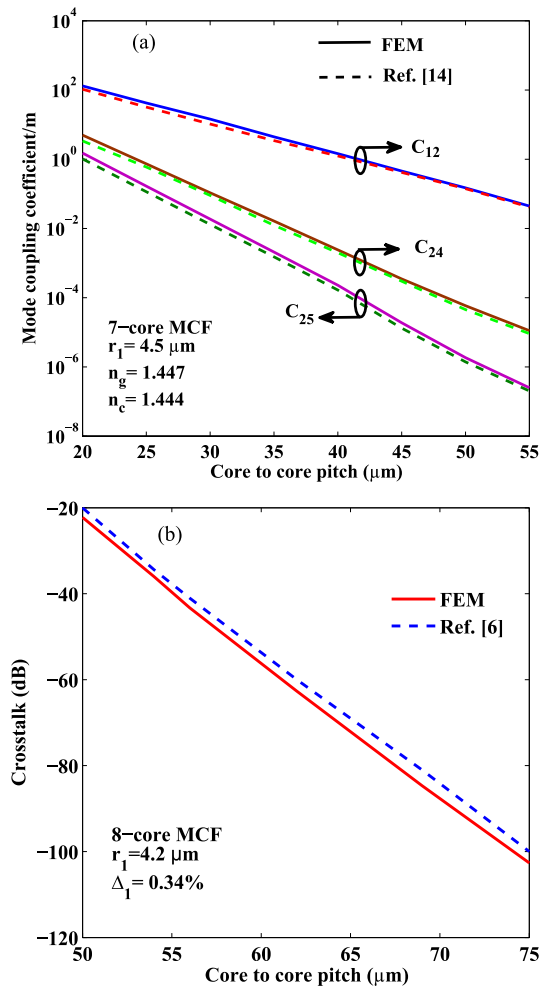


Fig. 3. (a) Mode coupling coefficients for a 7-core MCF. (b) XT in a homogeneous 8-core step-index MCF between core 1 and core 2.

Afterwards, the accuracy of the analytical formula given in (5) for intercore XT calculation is tested. A rectangular array 8-core MCF is used here as a model to carry out this comparison. The schematic cross section of the homogeneous 8-core MCF with step index profile is shown in Fig. 1(b). The cladding index is taken as 1.45 and the relative refractive-index difference between core and cladding is 0.34%, and the radii of the cores are  $4.2 \mu\text{m}$ . The index values and the radii are exactly the same as those in [6]. Variations of numerically simulated XT of step index 8-core MCF with  $\Lambda$  are shown in Fig. 3(b). In these simulations, the fiber length is taken as 100 m [6], and the wavelength  $\lambda$  of the optical signal is 1550 nm. The red solid line represents the XT between core 1 and core 2, which is obtained by using (5) and optical field from the rigorous vector  $\mathbf{H}$ -field FEM [31]. On the other hand, the blue dashed line relates the simulation results reported in [6]. The comparison of these results shown in Fig. 3(b) clearly demonstrates that the results obtained by using the FEM field and (5) matches very well with the results of [6]. The discrepancy between the crosstalk values is very small, which proves the feasibility of analytical formula used in this work.

After validating the computational accuracy of the numerical approaches developed, detailed analyses of 8-core MCF are carried out. Fig. 4(a) shows variations of coupling coefficients  $C_{mn}$  and coupling lengths  $L_c$  with core to core pitch  $\Lambda$  for a step index 8-core MCF, shown in Fig. 1(b). In this work, the radii of the cores are taken as  $4.45 \mu\text{m}$  and the relative

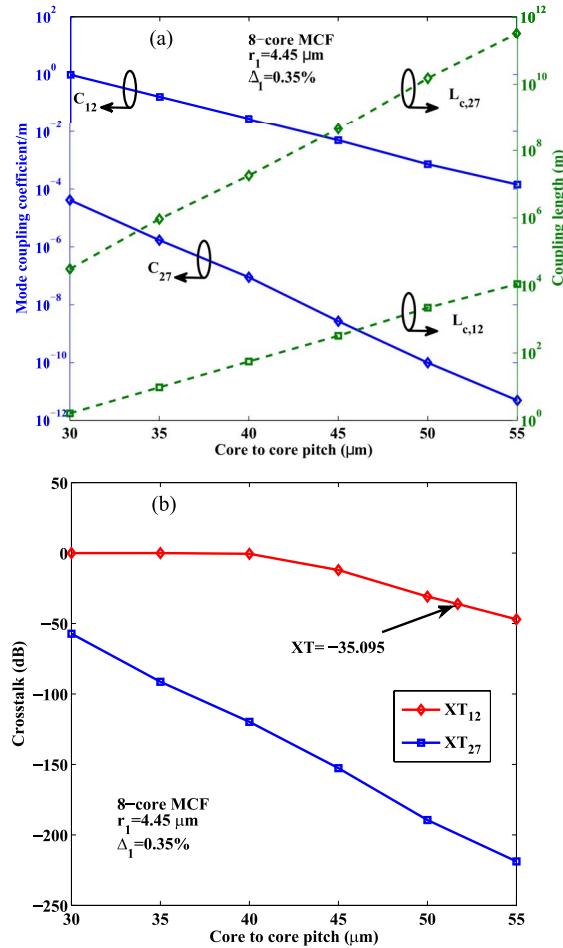


Fig. 4. (a) Mode coupling coefficients and coupling lengths for an 8-core MCF. (b) Variations of XT with core-to-core pitch for an 8-core MCF.

refractive-index difference between core and cladding as 0.35%, which are the structural parameters reported in the fabricated homogeneous 8-core MCF [22]. The blue solid lines represent the results of  $C_{mn}$ . On the other hand, the green dotted lines represent the results of  $L_c$ . The  $C_{mn}$  is determined by using the (1) and the accurate vector  $\mathbf{H}$ -field profile [31] to obtain the spatial overlap of the electromagnetic fields of the fundamental modes for each core in isolation. It can be observed from Fig. 4(a) that the  $C_{12}$  (coupling coefficient between core 1 and core 2) and  $C_{27}$  (coupling coefficient between core 2 and core 7) decreases with increase in  $\Lambda$ . It can also be noted that the coupling of power between core 2 and core 7 is much smaller compared to that between core 1 and core 2. The coupling length  $L_c$  for complete mode power transfer between the adjacent core can be calculated from their propagation constants, by  $L_c = \pi/2(\beta_e - \beta_o)$ , where  $\beta_e$  and  $\beta_o$  represents the propagation constants of the even and odd supermodes, respectively. Moreover, it can be observed in Fig. 1(b), that the cores are arranged in a two different rows with linear array of four cores. Thus, coupling length  $L_c$  can also be calculated by using the coupled mode theory, i.e.,  $L_c = \pi/2C_{mn}$  [32]. In this case,  $L_c$  calculated by both the approaches agreed very well. The results plotted in Fig. 4(a) shows that  $L_{c,12}$  and  $L_{c,27}$  increases with  $\Lambda$ , this is because  $L_c$  is inversely proportion to the  $C_{mn}$ . It is also known that  $L_c$  versus separation plotted in a semi-log scale yields a straight line, as shown here.

The  $C_{mn}$  and  $L_c$  serves as a measure for calculating the XT between the cores of MCF OI. The target XT level can be set to  $-35$  dB at 1550 nm for short reach MCF based OI

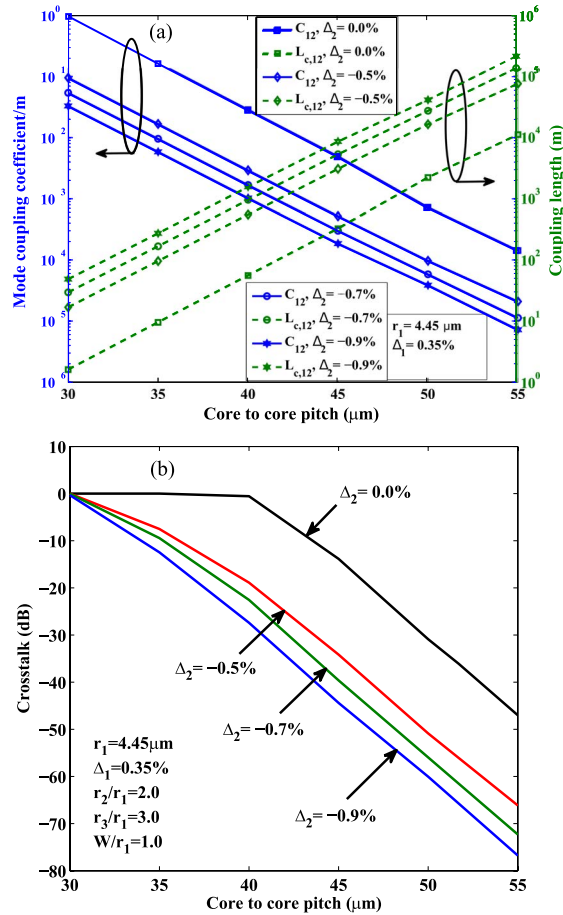


Fig. 5. (a) Variations of mode-coupling coefficient and coupling length with the core to core pitch for an 8-core TA-MCF for different  $\Delta_2$  values, when  $r_2/r_1 = 2.0$ ,  $r_3/r_1 = 3.0$ , and  $W/r_1 = 1.0$ . (b) Variations of XT with core-to-core pitch for an 8-core TA-MCF for different  $\Delta_2$  values.

transmission. Fig. 4(b) shows variations of XT calculated from (5) and by using accurate **H**-field profiles with core to core pitch  $\Lambda$  for a step index 8-core MCF. For the XT calculations, the fiber length  $L$  and the wavelength  $\lambda$  of the optical signal are taken as 100 m [6] and 1550 nm, respectively. The red solid line represents the result of  $XT_{12}$  (XT between core 1 and core 2). On the other hand, the blue solid line represents the result of  $XT_{27}$  (XT between core 2 and core 7). It can be observed from Fig. 4(b) that, as the value of  $\Lambda$  increases,  $XT_{12}$  has very small change at first and then decreases rapidly. On the other hand,  $XT_{27}$  decreases rapidly with increasing  $\Lambda$ . Fig. 4(b) clearly illustrates that the distance between the cores in the same row should be 51.7  $\mu\text{m}$  to achieve the target XT level of -35 dB. From the results depicted in Fig. 4(b), it can be concluded that the XT between core 2 and core 7 is very small and can be ignored for further simulation.

Earlier, trench-assisted structure was reported [14]–[16] as shown in Fig. 1(c) and next this is considered with the index profile given to suppress the power coupling between the cores of MCF. Fig. 5(a) illustrates the numerically simulated  $C_{12}$  and  $L_{c,12}$  of homogeneous TA-MCF OI with the  $\Lambda$  at a optical wavelength of 1550 nm where the relative trench position  $r_2/r_1$  and the relative trench width  $W/r_1$  are taken as 2.0 and 1.0, respectively and the core radius  $r_1$  and relative refractive-index difference between core and cladding are fixed at 4.45  $\mu\text{m}$  and 0.35%, respectively. The variations of  $C_{12}$  and  $L_{c,12}$  are simulated for  $\Delta_2 = -0.5\%$ ,  $-0.7\%$ , and  $-0.9\%$ . The  $C_{12}$  and  $L_{c,12}$  for normal step-index 8-core MCF structure is also included for comparison, which can be regarded as trench-assisted structure with  $\Delta_2 = 0\%$ , shown in Fig. 1(c). The blue

solid lines represent the results of  $C_{12}$ . On the other hand, the green dotted lines represent the results of  $L_{c,12}$  for different values of  $\Delta_2$ . The numerical results of  $C_{12}$  and  $L_{c,12}$  of 8-core TA-MCF OI are all simulated based on accurate **H**-field [31]. It can be observed from Fig. 5(a) that the  $C_{12}$  for homogeneous TA-MCF OI decreases with increase in  $\Lambda$  and exhibits very low  $C_{12}$  compared to step-index 8-core MCF. It can also be noted that the  $C_{12}$  decreases with increasing the value of low-index trench  $\Delta_2$ . When the  $\Lambda$  and  $\Delta_2$  is fixed at  $45 \mu\text{m}$  and  $-0.9\%$  respectively, then the simulated  $C_{12}$  and  $L_{c,12}$  are on the order of  $0.0001 \text{ m}^{-1}$  and  $10^4 \text{ m}$ , respectively. Fig. 5(a) clearly demonstrates that for higher value of low-index trench  $\Delta_2$  we can get the minimum  $C_{12}$  and maximum  $L_{c,12}$ . This shows the trench optically isolates the cores, reduces XT and increases the  $L_c$ .

Fig. 5(b) shows the variations of XT with  $\Lambda$  for 8-core homogeneous TA-MCF OI for  $\Delta_2 = -0.5\%$ ,  $-0.7\%$ , and  $-0.9\%$ . In order to compare the XT characteristics simulation results of step-index 8-core MCF structure is also included (shown here as  $\Delta_2 = 0\%$ ). The homogeneous TA-MCF OI parameters are same as that in Fig. 5(a) and  $XT_{12}$  is obtained by using (5). The plot shows that for a given  $\Delta_2$ ,  $XT_{12}$  decreases with increase in  $\Lambda$ . As can be seen from Fig. 5(b) that  $XT_{12}$  decreases with increasing the value of low-index trench  $\Delta_2$ . Moreover, for same  $\Lambda$  of  $45 \mu\text{m}$  and at the condition  $\Delta_2 = -0.5\%$ ,  $XT_{12}$  in TA-MCF OI is 20 dB smaller as compared to step-index counterpart. It can be noted from Fig. 5(b) that the  $XT_{12}$  reduces by more than 10 dB if low-index trench  $\Delta_2 = -0.9\%$  rather than  $\Delta_2 = -0.5\%$  is selected at  $\Lambda$  of  $45 \mu\text{m}$ . Fig. 5(b) clearly illustrate that the required  $\Lambda$  for a homogeneous TA-MCF OI is  $43.7 \mu\text{m}$  if the trench parameter  $\Delta_2$  is fixed at  $-0.7\%$ , corresponding to the target XT level of  $-35 \text{ dB}$ . On the other hand, the required  $\Lambda$  for a homogeneous TA-MCF OI is  $42.3 \mu\text{m}$  if the trench parameter  $\Delta_2$  is fixed at  $-0.9\%$ . This value is  $9.4 \mu\text{m}$  lower than the  $\Lambda$  required for step index 8-core MCF. However, the trench parameter  $\Delta_2$  of  $-0.7\%$  might be the limit for TA-MCF OI fabrication [16]. From this comparison, we can find clearly that the TA-MCF OI gives rise to better XT performance and arrangement can be more compact.

To clearly demonstrate the effect of trench on  $C_{mn}$ ,  $L_c$  and XT, dominant  $H_y$  field of the fundamental quasi-TE,  $H_{11}^y$  mode for 8-core step index and TA-MCF is plotted in Fig. 6(a). A rigorous vector **H**-field FEM [31] is employed to obtain the field distributions of trench index core for  $\Delta_2 = 0\%$ ,  $-0.5\%$ ,  $-0.7\%$  and  $-0.9\%$ , as shown in Fig. 1(c). It can be observed from Fig. 6(a) that the deployment of trench layer around each core can depress the field distributions, far away from the core. Variation of the modal field is plotted in a semi-log scale. Here outside the core (beyond  $r_1$ ) field varies exponentially, which is shown by a line with a constant slope when semi-log scale is used. The slopes between  $r_1$  to  $r_2$  and beyond  $r_3$  are the same as local index in these regions were same. However, when refractive index in the trench region, shown here between  $r_2$  and  $r_3$  is reduced, the slope of the field variation also shows faster field reduction. Moreover, field reduces faster between distance  $r_2 - r_3$  (where trench is located) if low-index trench  $\Delta_2$  is higher. Therefore, the spatial overlap of the electromagnetic field between two adjacent cores of TA-MCF OI will be small, resulting  $C_{mn}$  and XT will reduce even if the  $\Lambda$  is very small. It is shown in Fig. 6(a), as low-index trench  $\Delta_2$  is increased from  $-0.5\%$  to  $-0.9\%$ , a further reduction of  $C_{mn}$  and XT is possible.

Afterwards, in order to investigate the influence of the location of trench on  $L_c$  and XT characteristics, numerical simulations based on rigorous vector **H**-field FEM is illustrated in Fig. 6(b). Here, the fixed values for  $r_1$ ,  $\Delta_1$ ,  $\Lambda$ , and  $W/r_1$ , are assumed as  $4.45 \mu\text{m}$ ,  $0.35\%$ ,  $45 \mu\text{m}$ , and  $1.0$ , respectively and  $r_2/r_1$  varied from  $1.0$  to  $2.0$  to study the impact of the location of the trench layer. The simulations are carried out for  $\Delta_2 = -0.5\%$ ,  $-0.7\%$  and  $-0.9\%$ . It can be observed in Fig. 6(b), that the  $L_c$  increases with  $r_2/r_1$  and for a given location of the trench with high value of low-index trench  $\Delta_2$ . Moreover,  $XT_{12}$  of an 8-core homogeneous TA-MCF OI decreases with increasing  $r_2/r_1$  and for a given location of trench with high value of low-index trench  $\Delta_2$ . It can be noticed that, when  $\Lambda$  is fixed at  $45 \mu\text{m}$ , it is possible to obtain  $XT_{12}$  less than  $-35 \text{ dB}$  under two conditions—i)  $r_2/r_1 = 1.6$ ,  $\Delta_2 = -0.7\%$ , ii)  $r_2/r_1 = 1.4$ ,  $\Delta_2 = -0.9\%$ . Although the low-index trench  $\Delta_2 = -0.9\%$  may be preferable for XT reduction except for TA-MCF OI fabrication using

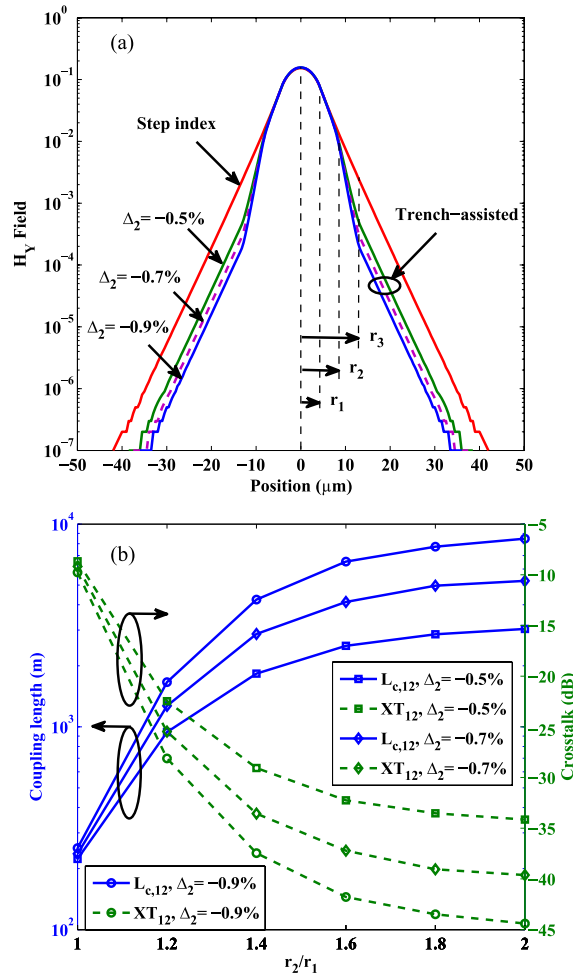


Fig. 6. (a)  $H_y$  field of the fundamental mode for 8-core step index and TA-MCF. (b) Variation of coupling length and XT with the  $r_2/r_1$  for an 8-core TA-MCF OI.

regular outside vapor deposition (OVD) and vapor axial deposition (VAD) processes, the  $\Delta_2$  value can be limited to be around  $-0.7\%$  [16]. Therefore, to find out the optimized arrangement of trench location with reduced  $\Delta$  and to make sure the trench is not overlapping with the adjacent trenches, we can increase the value of  $r_2/r_1$  to 2.0.

Fig. 7(a) shows the variations of XT with the  $\Delta_2$  for an 8-core TA-MCF OI for different  $W/r_1$  values. Here, the value for  $r_1$ ,  $\Delta_1$ ,  $\Delta$ , and  $r_2/r_1$  are fixed and assumed as  $4.45 \mu\text{m}$ ,  $0.35\%$ ,  $45 \mu\text{m}$ , and 2.0, respectively and  $\Delta_2$  is varied from 0% to  $-0.9\%$  to demonstrate the effect of trench width on XT properties. The numerical results of a XT for 8-core TA-MCF OI are simulated based on (5) and using accurate **H**-field profiles [31]. It can be observed from Fig. 7(a) that the XT between core 1 and core 2 of an 8-core homogeneous TA-MCF OI decreases with increasing the value of low-index trench  $\Delta_2$  for a given width of the trench layer. Moreover, the XT can be drastically reduced by employing larger width of the trench. It can be noted from Fig. 7(a) that, with  $\Delta_2 = -0.7\%$ , and  $\Delta_2 = 45 \mu\text{m}$ , XT reduces by more than 10 dB if  $W/r_1$  increased from 0.5 to 1.0. On the other hand, for the same value of  $\Delta_2 = -0.7\%$ , XT reduces by more than 28 dB if  $W/r_1$  is increased from 1.0 to 2.0. Moreover, if  $\Delta_2$  is fixed at  $-0.9\%$ , we can get XT of less than  $-80$  dB for  $W/r_1 = 2.0$  at  $\Delta = 45 \mu\text{m}$ .

Fig. 7(b) shows the variations of XT with the  $r_2/r_1$  for an 8-core TA-MCF OI for different  $W/r_1$ . Here, the value for  $r_1$ ,  $\Delta_1$ ,  $\Delta_2$ ,  $\Delta$  are fixed at  $4.45 \mu\text{m}$ ,  $0.35\%$ ,  $-0.9\%$ ,  $45 \mu\text{m}$ , respectively and  $r_2/r_1$  value is changed from 1.0 to 2.0 to demonstrate the effect of trench width on XT properties.

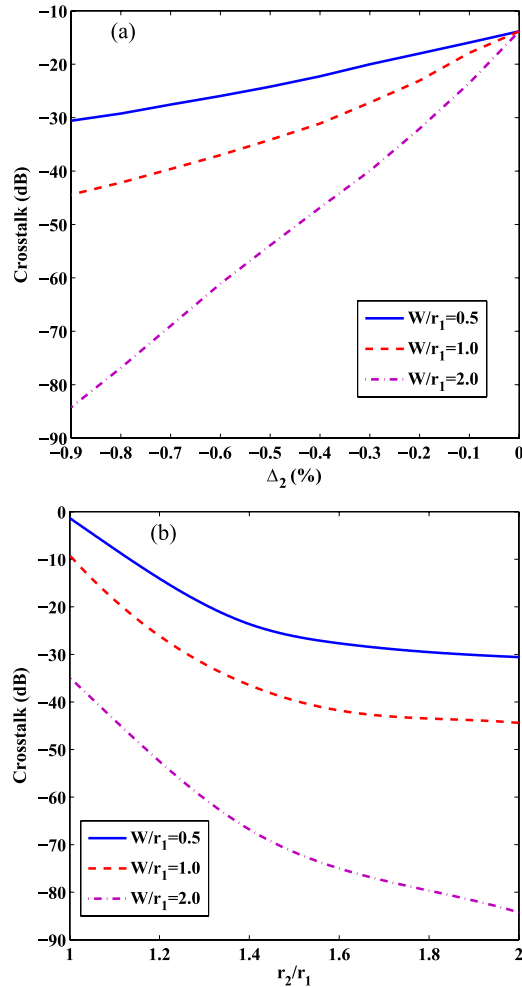


Fig. 7. (a) Variations of XT with the  $\Delta_2$  for an 8-core TA-MCF OI for different widths of the trench. (b) Variations of XT with  $r_2/r_1$  for an 8-core TA-MCF OI for different widths of the trench.

From the results depicted in Fig. 7(b), it can be inferred that the XT for an 8-core homogeneous TA-MCF OI decreases with increasing the value  $r_2/r_1$ . Moreover, the XT can be drastically improved by means of sufficiently large trench width. It can be noted from Fig. 7(b) that, with  $r_2/r_1 = 2.0$ , and  $\Lambda = 45 \mu\text{m}$ , XT reduces by more than 12 dB if  $W/r_1$  increased from 0.5 to 1.0. On the other hand, for the same value of  $r_2/r_1 = 2.0$ , XT reduces by more than 39 dB if  $W/r_1$  is increased from 1.0 to 2.0.

Afterwards, in order to design a more compact arrangement an 8-core heterogeneous TA-MCF OI is considered, where the delta of the core 2 is changed by 2% [see Fig. 1(b)]. Fig. 8 illustrates the variations of XT with  $\Lambda$  for an 8-core heterogeneous TA-MCF OI for  $\Delta_2 = -0.7\%$ ,  $r_2/r_1 = 1.3$ ,  $r_3/r_1 = 2.0$ , and  $W/r_1 = 0.7$ . In order to compare the XT characteristics simulation results of an 8-core homogeneous TA-MCF OI are also included. The homogeneous TA-MCF OI parameters are same as that in Fig. 5(b). It can be observed from Fig. 8 that the XT for heterogeneous TA-MCF OI decreases with increase in  $\Lambda$  and exhibits very low XT compared to 8-core homogeneous TA-MCF. It can also be noted that for same  $\Lambda$  of  $35 \mu\text{m}$  and with  $\Delta_2 = -0.7\%$ , XT in heterogeneous TA-MCF OI is 63 dB smaller as compared to homogeneous counterpart. Fig. 8 clearly illustrate that the required  $\Lambda$  for a heterogeneous step-index MCF OI is  $25.3 \mu\text{m}$ , corresponding to the target XT level of  $-35 \text{ dB}$ . On the other hand, the required  $\Lambda$  for a heterogeneous TA-MCF OI is  $22.1 \mu\text{m}$  if the trench parameter  $\Delta_2$  is fixed at  $-0.7\%$ . This

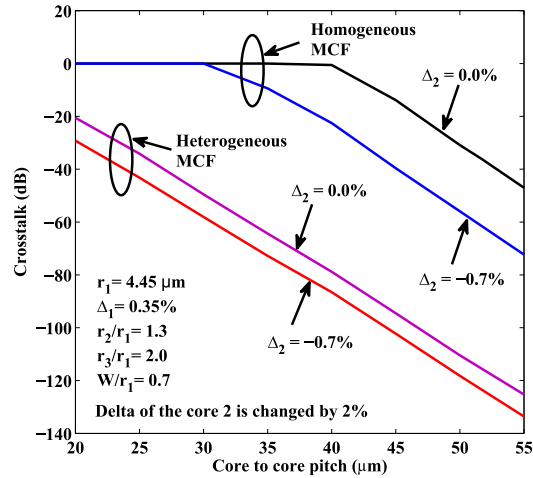


Fig. 8. Variations of XT with the core-to-core pitch for an 8-core heterogeneous TA-MCF when  $\Delta_2 = -0.7\%$ ,  $r_2/r_1 = 1.3$ ,  $r_3/r_1 = 2.0$ , and  $W/r_1 = 0.7$ .

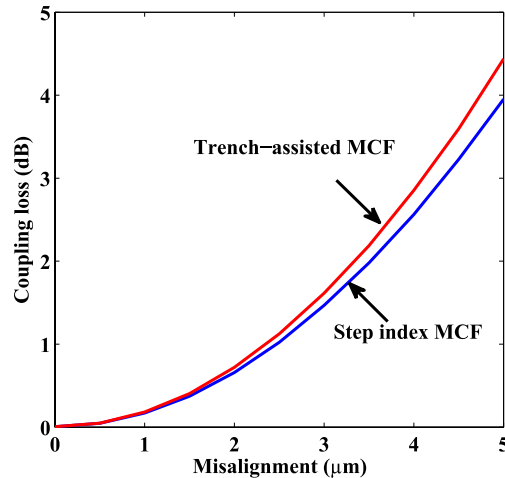


Fig. 9. Variations of coupling loss with misalignment for step-index MCF and TA-MCF OI.

value is  $21.6 \mu\text{m}$  lower than the  $\Lambda$  required for a homogeneous TA-MCF; therefore, the core arrangement can be more compact than MCF reported recently [6], [19], [23] with high density core for OI applications.

Whenever we couple a MCF to a standard SCF, it may not be perfectly aligned and effect of possible misalignment is studied next. Fig. 9 illustrates the variations of coupling loss caused by the misalignment for step index MCF and TA-MCF OI. Here, we fixed the value for  $r_1$ ,  $\Delta_1$ ,  $\Delta_2$ ,  $r_2/r_1$ ,  $r_3/r_1$ , and  $W/r_1$ , which are assumed as  $4.45 \mu\text{m}$ ,  $0.35\%$ ,  $-0.7\%$ ,  $1.3$ ,  $2.0$ , and  $0.7$ , respectively. Here, we still assume  $\Delta_2 = 0\%$ , shown in Fig. 1(c) for step index MCF. Simulations are based on full-vectorial modal **H**-field [31] and the LSBR [30] approach to accurately analyze the coupling loss on small variations in the facet's position along the optical axis of step index MCF and TA-MCF OI. In Fig. 9 the blue solid line represent the coupling loss for step index MCF and the red solid line represent the coupling loss for TA-MCF OI. It can be noticed that the 3 dB coupling loss for TA-MCF and step index MCF is obtained at the misalignment of  $4.1 \mu\text{m}$  and  $4.3 \mu\text{m}$ , respectively. As it can be observed in Fig. 9, coupling loss increases exponentially with misalignment for the both structure,  $\Delta_2 = 0\%$  and  $\Delta_2 = -0.7\%$ . However, for TA-MCF ( $\Delta_2 = -0.7\%$ ), the coupling loss is only slightly higher compared to step index MCF

( $\Delta_2 = 0\%$ ). This observed behavior can be explained by noting that trench assisted core increases the modal field confinement [see Fig. 6(a)] substantially. Therefore, the coupling losses increase moderately as the spot size decreases. It can also be noted that the coupling loss for step index MCF and TA-MCF OI are almost identical for misalignment of 0 to 1.2  $\mu\text{m}$ , which proves the feasibility of TA-MCF OI for their practical applications.

#### 4. Conclusion

A novel OI configuration based on 8-core heterogeneous TA-MCF is proposed for application in next generation exa-scale high performance computers and silicon photonic transceiver chips. A rigorous full-vectorial **H**-field FEM is used to calculate accurate modal field to obtain the coupling coefficient  $C_{mn}$  and coupling length  $L_c$  between the adjacent cores as a function of the important TA-MCF design parameters. The critical issue of crosstalk in the step index MCF and TA-MCF is quantified using the coupled power theory. In order to establish accuracy of this approach used here, comparisons are also made with the earlier reported results of 7-core hexagonal MCF and 8-core homogeneous MCF with same structural parameters. To design a TA-MCF OI, there are six important parameters that determine the profile— $r_1$ ,  $\Delta_1$ ,  $\Delta_2$ ,  $r_2/r_1$ ,  $\Lambda$ , and  $W/r_1$ . The impact of various TA-MCF OI design parameters on  $C_{mn}$ ,  $L_c$ , and XT are thoroughly investigated. Although, the low-index trench  $\Delta_2 = -0.9\%$  is preferable for XT reduction but in the view point of fabrication using regular OVD and VAD processes,  $\Delta_2 = -0.7\%$  is approximately suitable value. Through simulations, we have confirmed that OI based on 8-core heterogeneous TA-MCF can greatly reduce the crosstalk with more compact arrangement by adjusting the trench parameters. It is shown here that the required  $\Lambda$  for an 8-core homogeneous TA-MCF is 43.7  $\mu\text{m}$ , corresponding to the target XT level of  $-35$  dB. On the other hand, the required  $\Lambda$  in heterogeneous TA-MCF OI can be reduced to 22.1  $\mu\text{m}$ , if the parameters are fixed as  $r_2/r_1 = 1.3$ ,  $W/r_1 = 0.7$ , and  $\Delta_2 = -0.7\%$ .

Subsequently, the vector FEM is employed to obtain the modal propagation properties and the LSBR method is used to calculate the coupling loss caused by the misalignment between TA-MCF OI and SCF. The results are compared with the coupling loss between step index MCF and SCF to ascertain the trade off incurred by adding a trench layer to suit next generation OI specifications. The deployment of trench layer around each core increases the modal field confinement. Due to this fact, the spot size decreases and the coupling loss in TA-MCF OI is slightly higher than that of a step index MCF. This marginal increase in coupling loss can be traded off with drastic XT reduction in heterogeneous TA-MCF OI. The reported results clearly substantiate the potential of this technology for use in designing future practical OIs and silicon photonic transceivers.

---

#### References

- [1] M. A. Taubenblatt, "Optical interconnects for high-performance computing," *J. Lightw. Technol.*, vol. 30, no. 4, pp. 448–457, Feb. 2012.
- [2] S. Abrate *et al.*, "10Gbps POF ribbon transmission for optical interconnects," in *Proc. IEEE Photon. Conf.*, Arlington, VA, USA, Oct. 9–13, 2011, pp. 230–231.
- [3] J. A. Kash *et al.*, "Optical interconnects in future servers," presented at the Opt. Fiber Commun. Conf./Nat. Fiber Optic Eng. Conf., Los Angeles, CA, USA, Mar. 6–10, 2011, Paper OWQ1.
- [4] V. Francois and F. Laramée, "Multicore fiber optimization for application to chip-to-chip optical interconnects," *J. Lightw. Technol.*, vol. 31, no. 24, pp. 4022–4028, Dec. 2013.
- [5] J. K. Mishra, V. Priye, and B. M. A. Rahman, "Error probability performance of a short-reach multicore fiber optical interconnect transmission system," *Opt. Lett.*, vol. 40, no. 19, pp. 4556–4559, Oct. 2015.
- [6] M. J. Li, B. Hoover, V. N. Nazarov, and D. L. Butler, "Multicore fiber for optical interconnect applications," in *Proc. 17th Opto-Electron. Commun. Conf.*, Busan, South Korea, Jul. 2–6, 2012, pp. 564–565.
- [7] T. Morioka, Y. Awaji, R. Ryf, P. Winzer, D. Richardson, and F. Poletti, "Enhancing optical communications with brand new fibers," *IEEE Commun. Mag.*, vol. 50, no. 2, pp. s31–s42, Feb. 2012.
- [8] S. Matsuo *et al.*, "Crosstalk behavior of multi-core fiber with structural parameter drift in longitudinal direction," *IEICE Electron. Exp.*, vol. 8, no. 17, pp. 1419–1424, Sep. 2011.
- [9] S. Matsuo *et al.*, "Crosstalk behavior of cores in multi-core fiber under bent condition," *IEICE Electron. Exp.*, vol. 8, no. 6, pp. 385–390, Mar. 2011.

- [10] M. Koshihara, K. Saitoh, K. Takenaga, and S. Matsuo, "Analytical expression of average power-coupling coefficients for estimating intercore crosstalk in multicore fibers," *IEEE Photon. J.*, vol. 4, no. 5, pp. 1987–1995, Oct. 2012.
- [11] K. Takenaga, S. Tanigawa, N. Guan, S. Matsuo, K. Saitoh, and M. Koshihara, "Reduction of crosstalk by quasi-homogeneous solid multi-core fiber," presented at the Opt. Fiber Commun. Conf., San Diego, CA, USA, Mar. 21–25, 2010, Paper OWK7.
- [12] M. Koshihara, K. Saitoh, and Y. Kokubun, "Heterogeneous multi-core fibers: Proposal and design principle," *IEICE Electron. Exp.*, vol. 6, no. 2, pp. 98–103, Jan. 2009.
- [13] K. Saitoh, T. Matsui, T. Sakamoto, M. Koshihara, and S. Tomita, "Multi-core hole-assisted fibers for high core density space division multiplexing," in *Proc. 15th Opto-Electron. Commun. Conf.*, Sapporo, Japan, Jul. 5–9, 2010, pp. 164–165.
- [14] S. Zheng, G. Ren, Z. Lin, and S. Jian, "Mode-coupling analysis and trench design for large-mode-area low-cross-talk multicore fiber," *Appl. Opt.*, vol. 52, no. 19, pp. 4541–4548, Jul. 2013.
- [15] J. Tu, K. Saitoh, M. Koshihara, K. Takenaga, and S. Matsuo, "Design and analysis of large-effective-area heterogeneous trench-assisted multi-core fiber," *Opt. Exp.*, vol. 20, no. 14, pp. 15157–15170, Jul. 2012.
- [16] K. Saitoh, M. Koshihara, K. Takenaga, and S. Matsuo, "Crosstalk and core density in uncoupled multicore fibers," *IEEE Photon. Technol. Lett.*, vol. 24, no. 21, pp. 1898–1901, Nov. 2012.
- [17] J. Tu, K. Long, and K. Saitoh, "An efficient core selection method for heterogeneous trench-assisted multi-core fiber," *IEEE Photon. Technol. Lett.*, vol. 28, no. 7, pp. 810–813, Apr. 2016.
- [18] B. Li *et al.*, "The role of effective area in the design of weakly coupled MCF: Optimization guidance and OSNR improvement," *IEEE J. Sel. Topics Quantum Electron.*, vol. 22, no. 2, Mar./Apr. 2016, Art. no. 4401407.
- [19] T. Hayashi *et al.*, "125- $\mu\text{m}$ -Cladding 8-core multi-core fiber realizing ultra-high-density cable suitable for O-band short-reach optical interconnects," presented at the Opt. Fiber Commun. Conf., Los Angeles, CA, USA, Mar. 22–26, 2015, Paper Th5C.6.
- [20] B. G. Lee *et al.*, "End-to-end multicore multimode fiber optic link operating up to 120 Gb/s," *J. Lightw. Technol.*, vol. 30, no. 6, pp. 886–892, Mar. 2012.
- [21] D. L. Butler *et al.*, "Multicore optical fiber and connectors for high bandwidth density, short reach optical links," in *Proc. IEEE Opt. Interconnects Conf.*, Santa Fe, NM, USA, May 5–8, 2013, pp. 9–10.
- [22] T. Hayashi, T. Nakanishi, T. Sasaki, K. Saitoh, and M. Koshihara, "Dependence of crosstalk increase due to tight bend on core layout of multi-core fiber," presented at the Opt. Fiber Commun. Conf., San Francisco, CA, USA, Mar. 9–13, 2014, Paper W4D.4.
- [23] J. K. Mishra and V. Priye, "Design of low crosstalk and bend insensitive optical interconnect using rectangular array multicore fiber," *Opt. Commun.*, vol. 331, pp. 272–277, Nov. 2014.
- [24] K. Watanabe, T. Saito, K. Imamura, and M. Shiino, "Development of fiber bundle type fan-out for multicore fiber," in *Proc. 17th Opto-Electron. Commun. Conf.*, Busan, South Korea, Jul. 2–6, 2012, pp. 475–476.
- [25] Y. Abe, K. Shikama, S. Yanagi, and T. Takahashi, "Physical-contact-type fan-out device for multicore fibre," *Electron. Lett.*, vol. 49, no. 11, pp. 711–712, May 2013.
- [26] Y. Tottori, T. Kobayashi, and M. Watanabe, "Low loss optical connection module for seven-core multicore fiber and seven single-mode fibers," *IEEE Photon. Technol. Lett.*, vol. 24, no. 21, pp. 1926–1928, Nov. 2012.
- [27] Y. Ding, F. Ye, C. Peucheret, H. Ou, Y. Miyamoto, and T. Morioka, "On-chip grating coupler array on the SOI platform for fan-in/fan-out of MCFs with low insertion loss and crosstalk," *Opt. Exp.*, vol. 23, no. 3, pp. 3292–3298, Feb. 2015.
- [28] Y. Abe, K. Shikama, H. Ono, S. Yanagi, and T. Takahashi, "Fan-in/fan-out device employing v-groove substrate for multicore fibre," *Electron. Lett.*, vol. 51, no. 17, pp. 1347–1348, Aug. 2015.
- [29] T. Watanabe, M. Hikita, and Y. Kokubun, "Laminated polymer waveguide fan-out device for uncoupled multi-core fibers," *Opt. Exp.*, vol. 20, no. 24, pp. 26317–26325, Nov. 2012.
- [30] B. M. A. Rahman and J. B. Davies, "Analysis of optical waveguide discontinuities," *J. Lightw. Technol.*, vol. 6, no. 1, pp. 52–57, Jan. 1988.
- [31] B. M. A. Rahman and J. B. Davies, "Finite-element solution of integrated optical waveguides," *J. Lightw. Technol.*, vol. 2, no. 5, pp. 682–688, Oct. 1984.
- [32] K. Okamoto, *Fundamentals of Optical Waveguides*. Tokyo, Japan: Corona, 1992, ch. 4.
- [33] B. M. A. Rahman and J. B. Davies, "Vector-H finite element solution of GaAs/GaAlAs rib waveguides," *Proc. Inst. Elect. Eng. J.—Optoelectron.*, vol. 132, no. 6, pp. 349–353, Dec. 1985.